Environmental Science and Pollution Research (2021) 28:68834–68845
https://doi.org/10.1007/s11356-021-15440-x

RESEARCH ARTICLE

Enhanced dye-removal performance of Cu-TiO_2-fly ash composite by optimized adsorption and photocatalytic activity under visible light irradiation

Devagi Kanakaraju[1] · Muhamad Akif Aizuddin Jasni[1] · Andrea Pace[2] · Muhamad Hazim Ya[1]

Received: 1 April 2021 / Accepted: 9 July 2021 / Published online: 19 July 2021

Abstract

The performance of Cu/TiO_2/FA composite, a hybrid adsorbent-photocatalyst consisting of copper-doped titania particles supported on fly ash, was optimized, under visible light irradiation, for the removal of the model dye pollutant methyl orange (MO) by using a response surface methodology and Box-Behnken experimental design. Three independent variables were considered for the optimization study: catalyst/solvent dosage (0.5 – 2.0 g/L), irradiation time (30–120 min), and the initial concentration (5– 25 ppm) of the dye. A 99.91% rate of removal was achieved using 2 g/L dosage, 5 ppm initial concentration, and 100 min of irradiation time as the optimal operating conditions. The recorded trends support the hypothesis of a combined and synergic adsorption-photocatalytic degradation process which fully exploits the "capture and destroy" approach for pollutant removal.

Keywords Titanium dioxide · Photocatalysis · Wastewater · Doping · Degradation · Biomass

Introduction

The removal of organic pollutants from wastewater remains one of the major environmental challenge which, among others, includes the degradation of organic dyes frequently found in industrial wastewater (Baruah et al. 2020; Moztahida and Lee 2020; Jorfi et al. 2018; Talebi et al. 2017; Muhd Julkapli et al. 2014). Classical pollutant removal procedures include adsorption methods that use stable matrices that have a good affinity for the pollutant (Najafi et al. 2021). However, removal methods based only on adsorption are just shifting the problem from a contaminated fluid (the wastewater) to a contaminated solid (the pollutant@adsorbent). Alternatively, degradative methods, largely based on AOPs (Giwa et al. 2021), may take advantage of photocatalytic processes occurring over semiconductors such as titania (TiO_2) that eventually lead to pollutant mineralization (Chen et al. 2020). TiO_2 is one of the best photocatalysts for the degradation of organic pollutants in water; however, its use suffers from some drawbacks such as (i) inefficient exploitation of the visible light, (ii) low adsorption capacity for hydrophobic contaminants, (iii) fast recombination rate of electron-hole pairs, and (iv) troublesome post-treatment recovery of the TiO_2 nanoparticles from the treated water (Dong et al. 2015). Indeed, due to the wide bandgap of TiO_2 (3–3.2 eV), only a maximum absorption of 400 nm is absorbed (Gopinath et al. 2020). On the other hand, using a high titania/solvent ratio of TiO_2 nanoparticles in the solution will tend to form a suspension due to the instability of the nanosized TiO_2 particles, thus decreasing the light incident on the active centers and reducing the photocatalytic activity of TiO_2 (Dong et al. 2015; Andriantsiferana et al. 2014). In addition, poor affinity towards hydrophobic organic compounds implies low adsorption of a large variety of organic pollutants on the TiO_2 surface (Dong et al. 2015). Moreover, the fast recombination of photogenerated charge carriers causes a smaller amount of electron-hole pairs to be used efficiently in the photocatalytic reactions (Qian et al. 2021).

Responsible Editor: Sami Rtimi

✉ Devagi Kanakaraju
kdevagi@unimas.my

[1] Resource Chemistry Programme, Faculty of Resource Science and Technology, Universiti Malaysia Sarawak, 94300 Kota Samarahan, Sarawak, Malaysia

[2] Dipartimento di Scienze e Tecnologie Biologiche Chimiche e Farmaceutiche – STEBICEF, Università degli Studi di Palermo, Viale delle Scienze, Edificio 17, I-90128 Palermo, Italy

Currently, the most frequent ways of addressing these limitations include surface modifications of TiO_2 with other elements to extend TiO_2 absorption into the visible light region, and merging TiO_2 with other semiconductors (Adriana 2008; Cheng et al. 2020; Dong et al. 2015; Kumaravel et al. 2019; Qian et al. 2021), and supports (Shan et al. 2020; Xu et al. 2019). In our recent study (Kanakaraju et al. 2020), we extended the absorption range of titania by doping with copper, which was chosen as the metal dopant candidate due to its better performance compared to other transition metals (Etacheri et al. 2015; Pava-Gómez et al. 2018). Indeed, copper which possesses a narrow band gap for its oxides, such as CuO and Cu_2O with 1.4 eV and 2.2 eV, respectively, is less toxic and more abundant (Balık et al. 2019; Ganesh et al. 2014). Moreover, Cu as dopant increases the electron-hole pair separation efficiency, inhibits its recombination leading to a lifetime increase of the generated electrons, and subsequently improves photocatalytic activity even under visible light irradiation (Pedroza-Herrera et al. 2020). Several studies have reported the doping of Cu into TiO_2, which confirmed the improvement of photocatalytic efficiency of TiO_2 based on its application on pollutant removal (Ali et al. 2020; Shafei and Sheibani 2019; Delsouz Khaki et al. 2018; Ganesh et al. 2014; Aguilar et al. 2013).

In this context, the removal efficiency of photocatalytic processes can be improved by modifying the photocatalyst including adsorbing material that has the role of capturing the pollutant and bringing it close to the photocatalytic surface in a sort of a "catch and destroy" approach (Kanakaraju et al. 2018a) which requires the use of designed materials with specific functions as illustrated in Fig. 1.

Among adsorbent layers that could be used for this approach, alginate and chitosan have been widely studied due to their low environmental impact, given their "natural" origin. On the other hand, modern principles of circular economy are driving research toward the employment of waste reuse-recycling exploiting the properties of materials that could be obtained from industrial secondary products. With this scope, we recently explored the efficiency of fly ash (FA), a by-product of a local agroindustry, which was used as support for a Cu-doped TiO_2 photocatalyst (Kanakaraju et al. 2020). Indeed, FA, which possesses adsorbing capability based on its carbon content (Ahmed and Hand 2014), was used as the adsorbent phase in combination with semiconductors such as ZnO_2 (Pant et al. 2019), Bi_2O_3 (Luévano-Hipólito et al. 2019), and WO_3 (Visa et al. 2015a), as well as TiO_2 alone (Gilja et al. 2019; Visa et al. 2015b) or on polyurethane fibers (Joo Kim et al. 2014). However, UV irradiation was needed to achieve satisfying levels of pollutant removal, particularly when undoped titania was used as a photocatalyst. On the other hand, in previous studies where FA was used in combination with Cu-doped titania to increase the photocatalytic efficiency under visible light irradiation, the full Cu/TiO_2 coverage of spherical FA particles (as schematized in Fig. 2a) (Shijitha et al. 2009) or the high loading of doped photocatalyst on FA support (Fig. 2b) (Andronic et al. 2016) limited the possibility to take full advantage of FA adsorption capability.

This concept was confirmed by our recent study where SEM images of Cu/TiO_2/FA composites prepared from base-treated fly ash evidenced a lower loading of photocatalytic particles (Fig. 2c) with respect to composites prepared

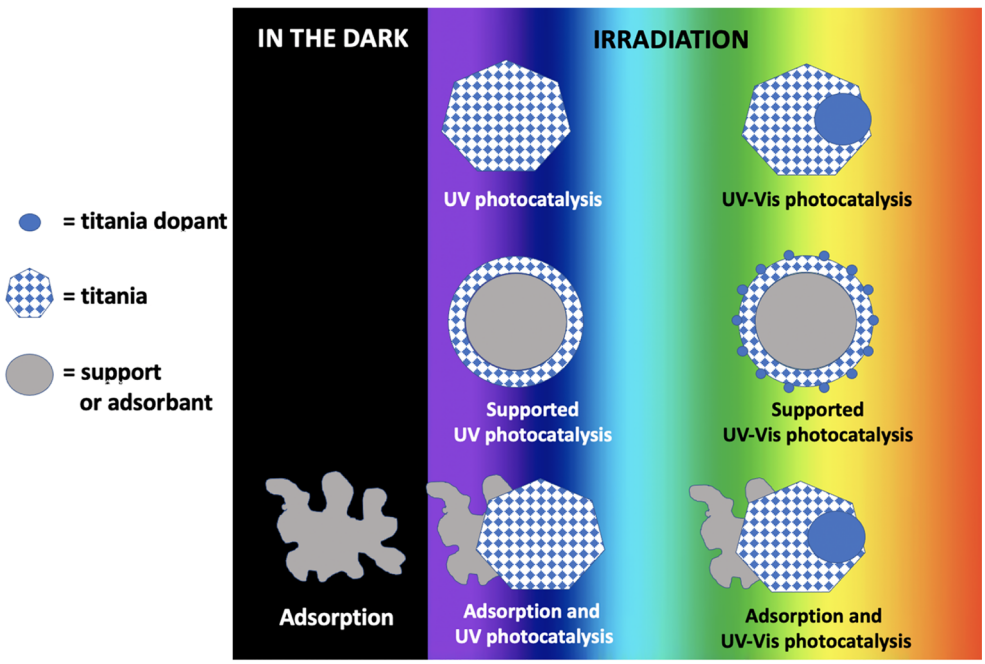

Fig. 1 Particle features, physical adsorption and photocatalytic degradation processes, and irradiation conditions involved in the removal of organic pollutants from aqueous solutions under heterogeneous conditions

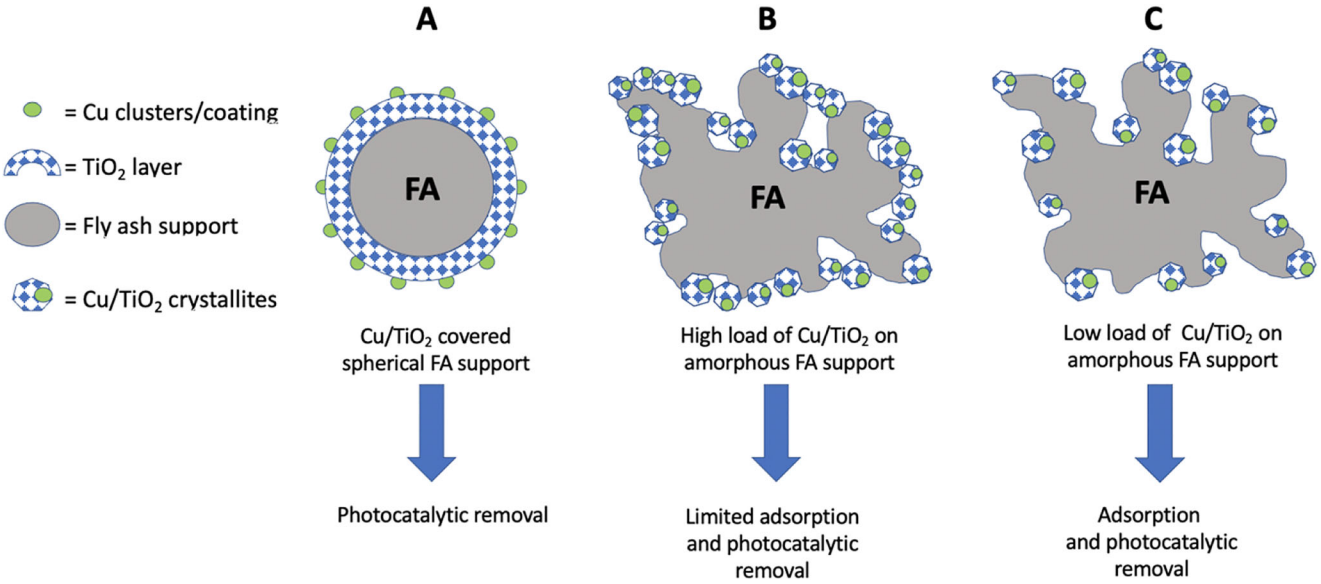

Fig. 2 Design of supported photocatalytic particles for combined adsorption/photodegradative removal of organic pollutants from water

from regular or acid-treated fly ash and showed the best dye-removal performance among prepared catalyst (Kanakaraju et al. 2020). Based on these considerations, we are now reporting an optimization study of the working conditions, using methyl orange (MO) as a model pollutant, to enhance the dye-removal performance of Cu/TiO_2/FA composites under visible light irradiation.

Materials and methods

Materials and reagents

Titanium (IV) butoxide and methyl orange (MO) were purchased from Sigma-Aldrich (USA). 2-Propanol, hydrochloric acid, and sodium hydroxide were purchased from Merck (Germany). Copper (II) nitrate trihydrate was obtained from Bendosen (Germany). Fly ash (FA) samples used in this study were collected from a sago factory located in Mukah, Sarawak, Malaysia.

Preparation of Cu/TiO_2/FA composite

TiO_2 was synthesized using our published sol-gel method with titanium (IV) butoxide as the precursor (Kanakaraju et al. 2017). Cu/TiO_2 (1:1 wt%) was then prepared by adding 1 g of TiO_2 into 100 mL of distilled water, followed by addition of 1 g of $Cu(NO_3)_2 \cdot 3H_2O$ under continuous stirring. Subsequently, the mixture was incubated at 90 °C for 3 h and left to cool at room temperature before filtration. The residue of Cu/TiO_2 was oven-dried at 105 °C for 2 h, followed by calcination in a furnace for 5 h at 300 °C resulting in a mint green–colored Cu/TiO_2 powder sample (Fig. 3).

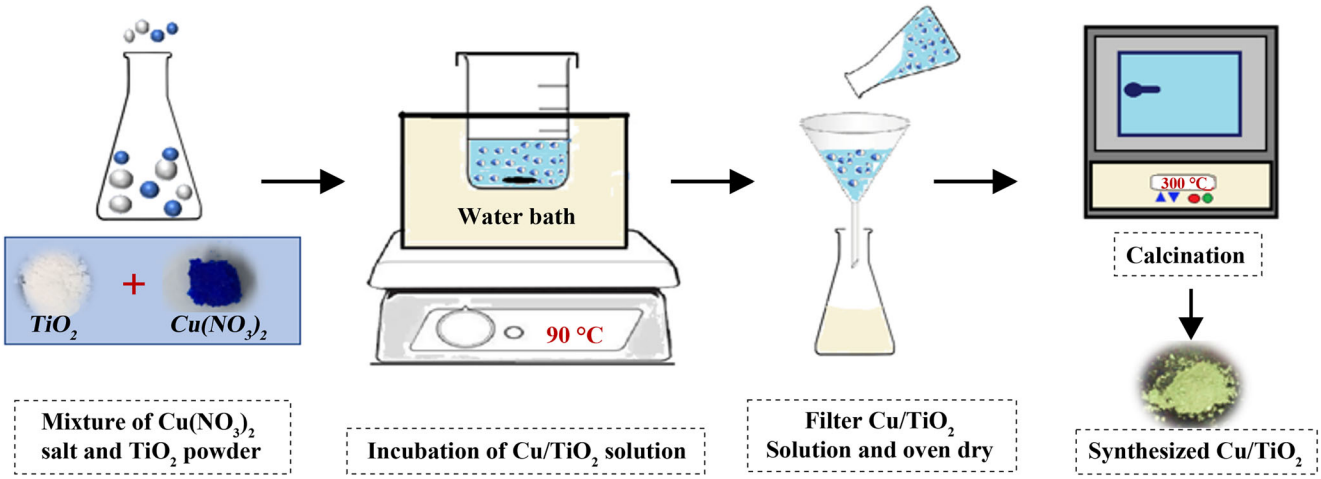

Fig. 3 Illustration of Cu-doped TiO_2 preparation process

FA was initially cleaned from undesired solid particles, such as sand and rock pieces prior to washing with distilled water. These pre-cleaned FA samples were then ground using a grinder (Quest Scientific FGR-350) to reduce the particle size. Subsequently, the grounded FA was sieved through a 500-μm sieve to obtain homogenized particles. The FA particles were initially suspended into 100 mL of 2 M aqueous NaOH solution, followed by washing (until a pH = 7 was reached in the washing solutions) and drying.

The Cu/TiO_2/FA composite was then produced by adapting a previously reported methodology (Kanakaraju and Wong 2018). Briefly, 1 g of Cu/TiO_2 was added to a beaker containing 100 mL of distilled water and 1 g of base-treated FA. The mixture was stirred continuously for 2 h, followed by filtration and drying in the oven at 100 °C. The obtained Cu/TiO_2/FA was applied for the dye degradation study.

Photocatalytic dye-removal procedures

The Cu/TiO_2/FA sample was investigated under different irradiation conditions to optimize its photocatalytic efficiency to degrade a model dye pollutant (MO) in aqueous solutions. A 1000 ppm MO solution was initially prepared by dissolving the dye powder (327.33 g/mol) in distilled water (1000 mL) and then diluted with water to obtain a 100 ppm stock solution. Such stock solution was further diluted to the desired initial concentration in 3 × 100 mL batches for each treatment condition. The initial concentration of MO for all degradation studies was fixed between at either 5, 15, or 25 ppm.

In a typical experiment, the Cu/TiO_2/FA photocatalyst was suspended in a 100 mL solution of MO in a 250-mL beaker (70-mm diameter) and kept in the dark for 30 min under continuous stirring to reach an adsorption-desorption equilibrium between the dye molecules and the surface of the photocatalyst particles (see process A in Fig. 4). After completion of the contact time in the dark, a sample (10 mL) was collected for analysis and the remaining solution mixture was irradiated at a distance of 17 cm from the top of the beaker, under either UVA (λ = 365 nm) or visible light (Opple, 4.5 W) for 2 h under continuous stirring. The samples were collected for analysis every 30-min interval for a duration of 2 h. The samples were centrifuged at 6000 rpm for 15 min and the resulting supernatant was analyzed using a UV-Vis spectrophotometer (Perkin Elmer, Lambda 25). The concentration of

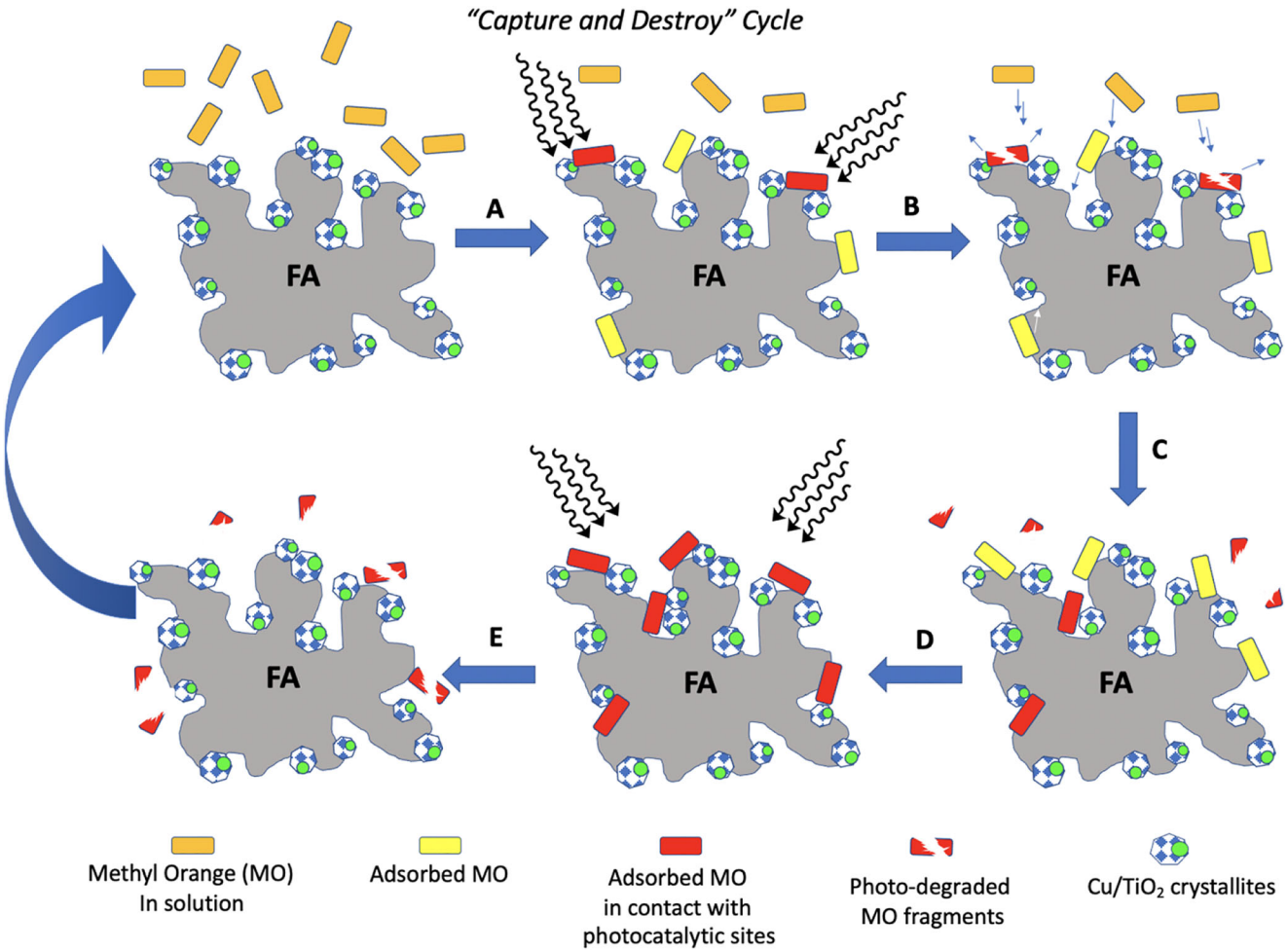

Fig. 4 The adsorption capability of the FA support after the photocatalytic degradation of the adsorbed MO pollutant

MO was measured at its maximum absorption wavelength (λ_{max} = 464 nm). The percentage of photocatalytic dye-removal (PDR) was calculated using Eq. 1:

$$PDR\ (\%) = \left(\frac{[MO]_0 - [MO]_t}{[MO]_0}\right) \times 100 \quad (1)$$

where $[MO]_0$ is the dye concentration recorded after 30 min contact time in dark and $[MO]_t$ is the concentration of dye solution after a given time (t) of irradiation.

Overall, the MO removal percentage, which takes into account both the adsorption and the photocatalytic degradation, is calculated by comparing the MO concentration recorded at a given irradiation time (t = 0–120) with the initial MO concentration C_i recorded before the adsorption contact time in the dark:

$$\text{MO Removal}\ (\%) = \left(\frac{C_i - [MO]_t}{C_i}\right) \times 100 \quad (2)$$

Results and discussion

Our previous study paved the way for the development of FA-supported photocatalysts taking advantage of both adsorption and photocatalytic processes for the degradative removal of organic pollutants in water (Kanakaraju et al. 2020; Kanakaraju and Wong 2018). To support the copper/titania catalyst, FA was previously treated with alkali to improve the functionality of raw FA surface area and pore structure (Chaudhary and Balomajumder 2014), thus lowering the load of Cu/TiO_2 crystallites (Fig. 2c) and maximizing the contribution of FA to the adsorption process. This approach fully exploits the "capture and destroy" cycle which refreshes the adsorption capability of the FA support after the photocatalytic degradation of the adsorbed pollutant (Fig. 4). This cycle consists of a combination of reversible equilibria and irreversible processes which are reciprocally connected and differently affected by several experimental parameters.

In particular, the initial adsorption equilibrium (step A in Fig. 4) controls the liquid/solid partition of methyl orange, where the concentration of adsorbed MO molecules ($[MO]_{ads} = C_i - [MO]_0$) accounts for both the molecule adsorbed on FA (yellow rectangles in Fig. 4) and the molecules in contact with the photoactive site supported on FA (red rectangles in Fig. 4). The following photocatalytic degradation (step B in Fig. 4) is an irreversible process whose outcome depends on the amount of "useful photons" (i.e., photons adsorbed by the photoactive site and producing the charge splitting required to degrade the pollutant) and is connected to previous step A by the amount of molecules in contact with photoactive site. Steps C and D are re-equilibration processes where fragments of degraded molecules detach from the particles, thus freeing spaces for more molecules to be adsorbed; additionally, mobility on the particle surface induces molecules adsorbed on FA to move closer to (or in contact with) the photoactive sites. Subsequent further photocatalytic degradation (step E) followed by the detachment of degraded molecules completes the cycle leaving the particle available to begin a new adsorption-photodegradation process.

On these bases, the entire "capture and destroy" cycle's efficiency will depend on several parameters such as the available surface on the FA particle, the contact time, the initial concentration of the pollutant, the catalyst/solvent ratio, the amount of photoactive sites, the wavelength, and irradiation time. Therefore, we decided to optimize the operating conditions of Cu/TiO_2/FA composite to degrade a MO aqueous solution, using a response surface methodology (RSM) and Box-Behnken design (BBD), which are successfully used to evaluate and optimize conditions in multiparametric experimental setups (Moztahida and Lee 2020; Talebi et al. 2017; Jin et al. 2014; Ferreira et al. 2007).

Response surface methodology analysis

Box-Behnken experimental design (BBD) was applied using Design Expert Software (version 7.1.6) to determine the optimum condition of MO removal using the Cu/TiO_2/FA photocatalyst. The chosen method was suitable for fitting a quadratic surface that helps optimize the operating parameters with a minimum number of experiments, including the analysis of the interaction between the parameters (Khosravi and Arabi 2016). In this design, a series of runs were completed by three independent variables, which include the catalyst/solvent dosage in the range 0.05–2.0 g/L, the irradiation time after the adsorption equilibration in the dark (30–120 min), and the initial concentration (C_i) of the dye (5–25 ppm). All the optimization experiments were conducted under visible light irradiation (λ = 400 to 700 nm). The samples were withdrawn at a specific contact time as suggested by the RSM design matrix. The factorial levels were coded as −1 (low), 0 (medium), and 1 (high). Table 1 summarizes the experimental range and the level of independent variables considered for MO removal while Table 2 shows the 15 BBD experiments set up with the ranges and levels in code unit.

The data gained on the dependent variable (photocatalytic MO removal percentage) from the experimental results were fitted to a polynomial equation to quantify the curve effects. The resulting equation was generated in terms of the coded values and is expressed in Eq. 2:

Table 1 The range and levels of independent variables for photocatalytic MO removal

Variables	Coded	Range variables		
		−1	0	1
Initial concentration (ppm)	A	5	15	25
Irradiation time (min)	B	30	75	120
Photocatalyst dosage (g/L)	C	0.5	1.3	2.0

$$PDR\ (\%) = 69.28–18.48A–1.35B + 25.29C + 1.30AB + 6.80AC + 4\ 85\mathrm{BC} + 4.33A^2 + 7.74B^2–10.36C^2 \quad (\mathrm{I3})$$

where, PDR is percentage of photocatalytic dye removal (see also eq. 1), and A, B, and C are coded values for the initial concentration of MO, irradiation time, and adsorbent dosage, respectively.

Statistical analysis

The obtained photocatalytic removal efficiencies varied from 13.07 to 99.91% (Table 3) and the predicted values well fitted the experimental results as shown in Fig. 5 where the linear regression between predicted and recorded values resulted in a good correlation ($R^2 = 0.99$).

Moreover, based on the ANOVA analysis, model F-value of 1949.98 implied that the model has a significant effect on the response (Table 4). This means that the "model F-value" has less than 0.01% probability for noise to occur. p-value was used to estimate whether F was large enough to indicate statistical significance. The p-value (prob>F) was less than 0.05, which indicates that the quadratic model was statistically significant (Körbahti and Tanyolaç 2008).

Furthermore, the "Lack of Fit F-value" of 0.37 with p>0.05 indicates that the "Lack of Fit" was not significant relative to the pure error in the model, thus indicating an accepted model. The well-fitted model was obtained for the equation of percentage removal (Eq. 3). In addition, the R^2 of 0.9997, adjusted R^2 of 0.9992, and predicted R^2 of 0.9980 showed that the experimental result fitted the polynomial model adequately (Table 4) (Khosravi and Arabi 2016). The adequate precision, which measures the signal to noise ratio and where a ratio greater than 4 is desirable (Arslan-Alaton et al. 2009), was 150.622 for our model (Table 4) demonstrating the significance and adequacy of the employed model (Kaushik and Malik 2011). Finally, the coefficient variation (CV) value of 1.01 for our model indicates good precision and reliability of the experiments performed (Kanakaraju et al. 2018b).

Model interpretation

A graphical representation of the model expressed by Eq. 3 is illustrated in Fig. 6, where the photocatalytic removal percentage is reported in 3D surface plots as a function of pairs of independent variables.

Effect of initial dye concentration and irradiation time

The effect of C_i (5–25 ppm) and t (30–120 min) was investigated using a fixed dosage of 1.3 g/L of Cu/TiO_2/FA (Fig. 6a). The percentage removal of MO decreased at a high initial concentration (25 ppm) from 65.41% at 30 min to 60.23% at 120 min. This could be explained by considering that, at a higher initial concentration, a greater number of MO molecules would

Table 2 RSM for three independence variables in corresponding natural value and codes unit of photocatalytic MO removal

Run	Independent variables			Coded variables		
	Initial concentration (ppm)	Contact time (min)	Adsorbent dosage (g/L)	*A*	*B*	*C*
1	15	75	1.3	0	0	0
2	5	30	1.3	−1	−1	0
3	25	120	1.3	1	1	1
4	25	75	0.5	1	0	−1
5	25	75	2.0	1	0	1
6	15	75	1.3	0	0	1
7	15	120	0.5	0	1	−1
8	25	30	1.3	1	−1	0
9	5	75	0.5	−1	0	−1
10	15	30	2.0	0	−1	1
11	5	75	2.0	−1	0	1
12	5	120	1.3	−1	1	0
13	15	120	2.0	0	1	1
14	15	30	0.5	0	−1	−1
15	15	75	1.3	0	0	0

Table 3 Experimental values and predicted values by the experimental model designed by BBD

Standard order	Variables			MO removal	
	Initial concentration (ppm)	Contact time (min)	Adsorbent dosage (g/L)	Predicted values (%)	Experimental result (%)
1	5	30	1.3	99.88	99.90
2	25	30	1.3	65.53	65.41
3	5	120	1.3	99.80	99.91
4	25	120	1.3	60.23	60.23
5	5	75	0.5	63.25	63.52
6	25	75	0.5	12.69	13.07
7	5	75	2.0	100.23	99.85
8	25	75	2.0	76.86	76.59
9	15	30	0.5	47.86	47.31
10	15	120	0.5	35.18	34.79
11	15	30	2.0	88.45	88.84
12	15	120	2.0	95.46	95.73
13	15	75	1.3	69.28	70.29
14	15	75	1.3	69.28	68.56
15	15	75	1.3	69.28	68.99

quickly saturate the available binding sites on the surface area of photocatalyst Cu/TiO_2/FA. In addition, high initial concentration of MO also reduces light intensity from penetrating the solution, thus reducing the catalytic activity (Anwer et al. 2019). In this context, where dye degradation is slow, support (FA) degradation could occur partially, releasing part of the initially adsorbed dye back into solution. This effect was counterbalanced by fast dye degradation occurring at lower C_i. Indeed, the highest MO removal (99.91%) was obtained using 5 ppm of MO at a contact time of 120 min.

Effect of irradiation time and catalyst/adsorbent dosage

The combined effect of irradiation time (30–120 min) and catalyst dosage (0.5–2.0 g/L) was investigated using an initial MO

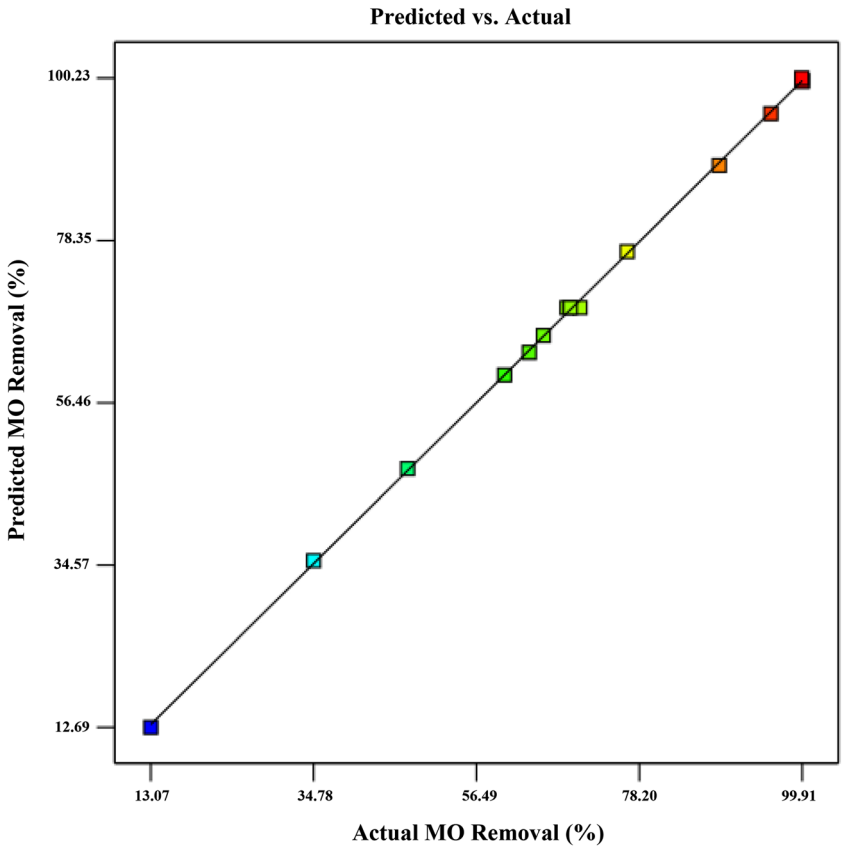

Fig. 5 Predicted versus experimental values of MO removal (R^2 = 0.99) by Cu/TiO_2/FA

Table 4 ANOVA for photocatalytic MO removal percentage using Cu/TiO_2/FA

Source	Sum of squares	Degree of freedom (df)	Mean square	*F* value	*p*-value Prob> *F*	
Model	8893.02	9	988.11	1949.98	< 0.0001	Significant
A	2732.82	1	2732.82	5393.05	< 0.0001	
B	14.53	1	14.53	28.67	0.0031	
C	5116.67	1	5116.67	10097.43	< 0.0001	
AB	6.79	1	6.79	13.39	0.0146	
AC	184.82	1	184.82	364.74	< 0.0001	
BC	94.19	1	94.19	185.87	< 0.0001	
A^2	69.35	1	69.35	136.85	< 0.0001	
B^2	221.41	1	221.41	436.94	< 0.0001	
C^2	396.01	1	396.01	781.50	< 0.0001	
Residual	2.53	5	0.51			
Lack of fit	0.91	3	0.30	0.37	0.7844	Not significant
Pure error	1.62	2	0.81			
Cor total	8895.56	14				

R^2 = 0.9997, Adj R^2 = 0.9992, Pred R^2 = 0.9980, Adeq Precision = 150.622, CV = 1.01

concentration of C_i = 15 ppm. The removal efficiency of MO increased with the irradiation time at a higher catalyst dosage (red part of the surface; Fig. 6b) due to the more prolonged photocatalytic degradation. Analogously, at a fixed irradiation time, the increase in adsorbent dosage from 0.5 to 2.0 g/L caused an increase in MO removal due to the availability of more adsorption and photoactive sites for the absorption and degradation of MO molecules (Anwer et al. 2019; Carp et al. 2004). On the other hand, an increase of irradiation time at low adsorbent dosage may cause partial degradation of the FA support, thus decreasing the initial removal rate until, for prolonged times (>75 min), the photocatalytic process prevails due to the still active photocatalytic particles.

Effect of catalyst dosage and initial dye concentration

The combined effects of catalyst/solvent ratio and C_i were investigated at a fixed irradiation time of 75 min (Fig. 6c). The graphic clearly illustrates the positive combined effect of high catalyst/adsorbent dosage and low initial concentration in determining the performance of MO removal that was practically quantitative (99.85%) at C_i = 5 ppm and catalyst dosage of 2.0 g/L. At the opposite corner (dark blue in Fig. 3c), the graph showed the combined deleterious effect of high Ci and low catalyst loading, resulting in the lowest recorded MO removal of 13.07%, likely due to active site saturation (Gaya and Abdullah 2008). On the other hand, an increase in catalyst loading would make more sites available thus increasing the removal rate (Reza et al. 2017). Similarly, a decrease in pollutant concentration would not saturate the active sites thus rendering the "capture and destroy" cycle more efficient. In fact, despite the cycle involving particle regeneration after completing the last degradation step, a larger amount of pollutant to treat would make such regeneration process slower.

Assessment and validation of optimized conditions

To assess the optimized operating conditions to maximize the dye removal performance of Cu/TiO_2/FA composite, the three independent variables were set as "in range" while MO removal percentage was set as the "target." The analysis was performed based on the RSM predicted values and, under optimized conditions, a 99.91% of MO removal was attained (Table 5).

Such conditions were further tested under other "blank" conditions (e.g., dark condition, solution irradiation, as well as irradiation with fly ash, undoped TiO_2, or Cu/TiO_2 suspensions) to compare their efficiency under either UVA or visible light irradiation. The trend lines illustrated in Fig. 7 show the contribution of both adsorption and photocatalytic removal, and the overall MO removal was calculated according to Eq. 2, using the initial concentration C_i as a reference and taking into account also of the equilibration period in the dark (shown as negative time range (t = −30 to 0 min)).

The photolysis effect on MO solution under both light sources showed minimal removal ranging from 6.76 to 10.03% (Fig. 7 a, b). The Cu/TiO_2-doped sample showed 54.32% MO removal while undoped TiO_2 produced only 11.59% under visible light. On the other hand, undoped TiO_2 efficiently removed 89.53% under UV light while Cu/TiO_2 also resulted in a slightly lower removal (70.27%) under similar conditions. The removal of MO using base-FA was

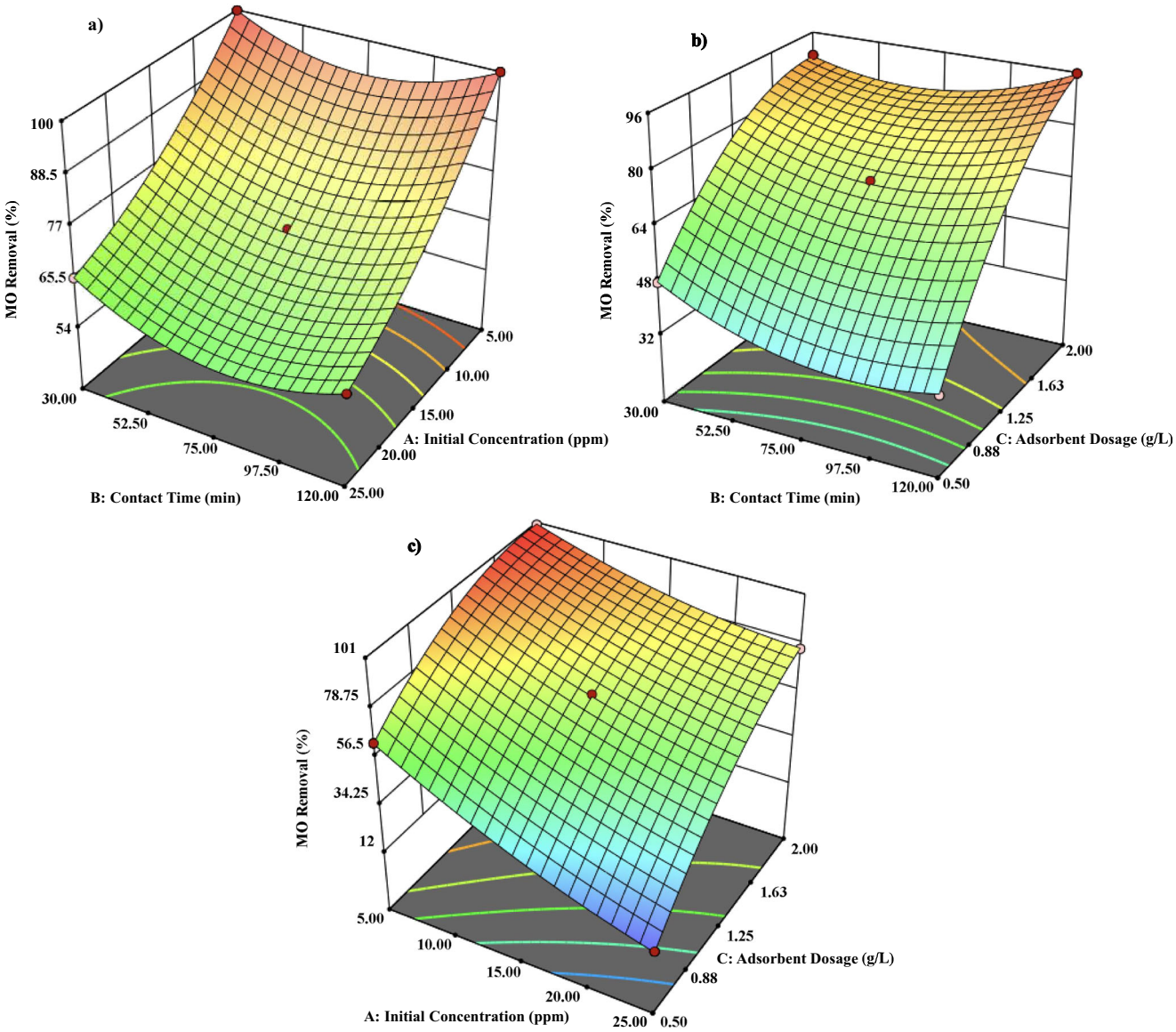

Fig. 6 3D surface plot of photocatalytic MO removal percentage using Cu/TiO_2/FA as a function of a irradiation time and initial dye concentration, b catalyst/adsorbent dosage and irradiation time, c catalyst/adsorbent dosage and initial dye concentration

96.78% and 89.54% under UV and visible irradiation, respectively; however, no significant improvement of the removal is observed during the irradiation time, supporting the hypothesis that the adsorption effect by based-treated FA strongly contributes to the physical removal of MO, but not to its photocatalytic degradation. Overall, the Cu/TiO_2/FA showed the best combined adsorption-photocatalytic performance with a complete MO removal when assessed under optimized RSM conditions using either UV or visible light sources.

Photocatalytic MO removal mechanism over Cu/TiO_2/FA composite

The photocatalytic performance of Cu/TiO_2/FA is linked to the abundance of oxygen vacancies and to the presence of Cu species able to capture the photogenerated electron, thus limiting counterproductive e^-/h^+ recombination processes (Xin et al. 2008). Moreover, the higher amount of hydroxyl groups on the surface of Cu/TiO_2 with respect to the undoped TiO_2

Table 5 Optimized conditions by RSM for MO removal using Cu/TiO_2/FA

Adsorbent dosage (g/L)	Initial concentration (ppm)	Contact time (min)	Photocatalytic MO removal (%)	
			Predicted	Actual
2.0	5	100	99.27	99.91

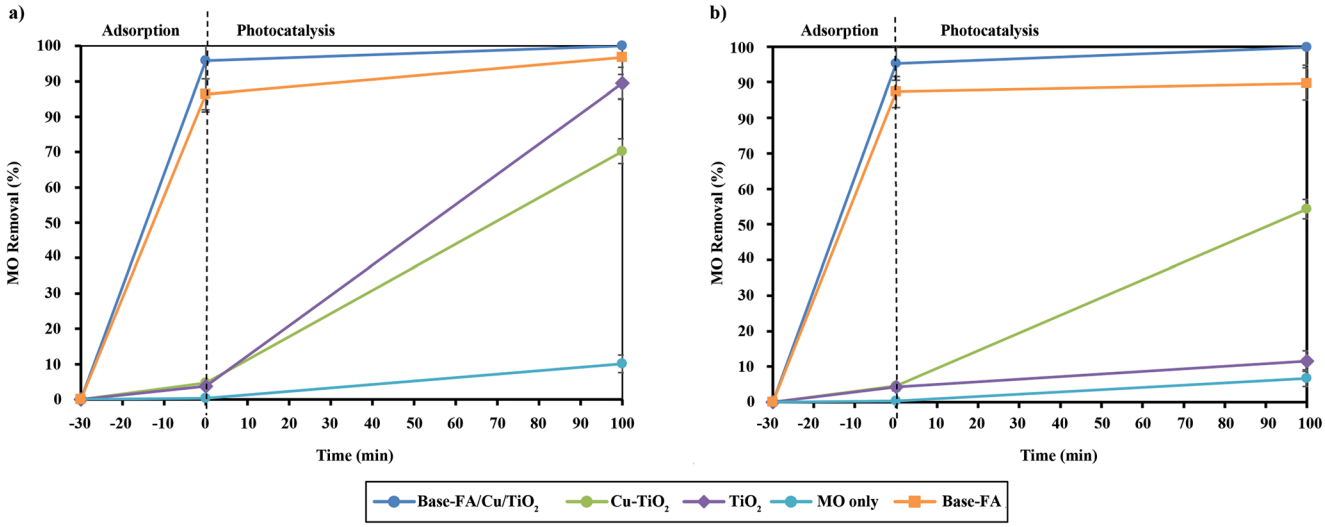

Fig. 7 Percentage of overall MO removal using various samples under optimized operating condition assessed by RSM under different light sources: **a** UV light, **b** visible light

would contribute to improving the photocatalytic activity. Considering the rapid MO adsorption process and the fact that irradiation starts after 30 min in the dark, allowing most of the MO molecules to be adsorbed on the Cu/TiO_2/FA particles, the contribution of the solution photodegradation of MO to the removal process can be neglected.

On the Cu/TiO_2/FA particle, the photocatalytic mechanism of MO removal involves a variety of competing processes that depend on the electronic properties (and valence state) of the Cu/TiO_2 clusters, as well as on the redox potential of MO and its excited state MO*.

The type of copper species in the system, e.g., Cu_2O or CuO, affects the bandgap and the electron (or hole) transfer that follows light absorption (Rtimi et al. 2017; Abidi et al. 2019). Consequently, also the type of irradiation would affect the mechanism of photocatalytic MO removal since only Cu_xO species could be excited under visible light (Eq. 4), while both Cu_xO and TiO_2 might concur in electron/hole photogeneration under ultraviolet irradiation (Eq. 5) (Yu et al. 2019).

$$Cu/TiO_2/FA + h\nu\ (visible\ light) \rightarrow CuxO(h^+) + CuxO(e^-) \quad (4)$$

$$Cu/TiO_2/FA + h\nu\ (ultraviolet\ light) \rightarrow TiO2\ (h^+) + TiO2(e-) + CuxO(h+) + CuxO(e^-) \quad (5)$$

When MO concentration is higher than 1.6×10^{-4} M, MO can be reduced (by electrons in the conduction band) at −0.28 eV or oxidized (by hole in the valence band) at a potential of +1.4 eV, thus efficiently competing with water in the hole scavenging process (Yu et al. 2012).

In our system, the maximum initial MO concentration in solution is 25 ppm (7.6×10^{-5} M) but the local concentration of MO adsorbed on the photocatalytic particle is much higher than the nominal solution concentration. Therefore, the photocatalytic degradation mechanism occurring on the adsorbed MO (MO_{ads}) molecules (steps B or E of the cycle illustrated in Figure 4) should mostly involve direct CB (e^-) and VB (h^+) redox processes. Given the energy content of photogenerated electrons and holes, both types of conduction band electrons, i.e., TiO_2 (e^-) or Cu_xO(e^-), would be able to trigger the reductive degradation of adsorbed MO (Eq. 6). At the same time, only TiO_2 (h^+) or CuO (h^+) would be reduced by MO during its oxidative degradation (Eq. 7). On the other hand, superoxide and hydroxyl radical mediated processes would be responsible for the oxidation of residual MO molecules in solution (MO_{sln}) (Eqs. 8–11).

$$TiO_2\ (e-)\ or\ Cu_xO(e^-) + MO_{ads} \rightarrow TiO_2\ or\ Cu_xO + MO\ reductive\ degradation\ products \quad (6)$$

$$TiO_2\ (h^+)\ or\ Cu_xO(h^+) + MO_{ads} \rightarrow TiO_2\ or\ Cu_xO + MO\ oxidative\ degradation\ products \quad (7)$$

$$TiO_2\ (e^-)\ or\ Cu_xO(e^-) + O_2 \rightarrow TiO_2\ or\ Cu_xO + O_2{-}(superoxide\ radical\ anion) \quad (8)$$

$$O_2^- + H_2O \rightarrow \cdot OOH\ (hydroperoxyl\ radical) + OH^- \quad (9)$$

$$TiO_2\ (h^+)\ or\ Cu_xO(h^+) + H_2O \rightarrow TiO_2\ or\ Cu_xO + H^+ + \cdot OH\ (hydroxyl\ radical) \quad (10)$$

$$OOH\ or \cdot OH + MO_{sln} \rightarrow MO\ oxidative\ degradation\ products \quad (11)$$

In addition, since MO itself is capable of light absorbing (especially at the beginning of the irradiation when the adsorbed MO concentration is at its maximum), the excited MO* could inject an electron into the conduction band of the semiconductor particle thus producing the reactive species involved in either Eq. 6 or Eq. 8 and, at the same time, a partially oxidized MO radical cation that could undergo further oxidative degradation (Eqs. 12–14).

$$MO + h\nu \rightarrow MO^* \quad (12)$$

$$MO^* + TiO_2 \text{ or } Cu_xO \rightarrow TiO_2\ (e^-) \text{ or } Cu_xO(e^-) + MO^+ \ (\text{oxidized MO radical cation}) \quad (13)$$

$$MO^+ \rightarrow\rightarrow MO \text{ oxidative degradation products} \quad (14)$$

Conclusion

The efficiency of Cu/TiO_2/FA photocatalyst on the removal of MO was investigated. A general trend was noted whereby at fixed irradiation times, increasing the catalyst dosage and decreasing the dye concentration work in synergy to improve the removal performance of the catalyst. In real cases, where the initial pollutant concentration cannot be chosen or adjusted, increasing both irradiation time and catalyst loading maximizes the photocatalytic degradation process. The preliminary base treatment of the raw fly ash support is crucial to roughen the particle surface with cavities and irregularities where the photoactive Cu/TiO_2 particles can reside and the pollutant can be adsorbed. Overall, the combination of physical processes (adsorption) and (photo)chemical processes (degradation) allow for a better removal performance by following the "capture and destroy" approach.

Author contribution Devagi Kanakaraju involved in research grant acquisition, research project administration, experimental design, supervision, interpretation of data, and revising the manuscript. Muhamad Akif Aizuddin bin Jasni contributed to performing experiments, data analyses, and writing the manuscript. Andrea Pace contributed in reviewing the manuscript and interpretation of data. Muhamad Hazim bin Ya conducted synthesis of samples, data collection, and data analyses.

Funding This work was supported by the Universiti Malaysia Sarawak under the Tun Openg Chair (F07/ TOC/1737/2018).

Data availability Not applicable.

Declarations

Ethics approval and consent to participate Not applicable.

Consent for publication Not applicable.

Competing interests The authors declare no competing interests.

References

Abidi M, Assadi AA, Bouzaza A, Hajjaji A, Bessais B, Rtimi S (2019) Photocatalytic indoor/outdoor air treatment and bacterial inactivation on Cu_xO/TiO_2 prepared by HiPIMS on polyester cloth under low intensity visible light. Appl Catal B Environ 259:118074

Adriana Z (2008) Doped-TiO_2: A Review. Recent Pat Eng 2:157–164

Aguilar T, Navas J, Alcántara R, Fernández-Lorenzo C, Gallardo JJ, Blanco G, Martín-Calleja J (2013) A route for the synthesis of Cu-doped TiO_2 nanoparticles with a very low band gap. Chem Phys Lett 571:49–53

Ahmed ZT, Hand DW (2014) Quantification of the adsorption capacity of fly ash. Ind Eng Chem Res 53:6985–6989

Ali Z, Shah AU, Ali Z, Mahmood A (2020) Influence of Cu modified surface states by sol gel technique on photocatalytic activity of titanium dioxide. Mater Chem Phys 249:123169

Andriantsiferana C, Mohamed EF, Delmas H (2014) Photocatalytic degradation of an azo-dye on TiO_2/activated carbon composite material. Environ Technol (United Kingdom) 35:355–363

Andronic L, Isac L, Miralles-Cuevas S, Visa M, Oller I, Duta A, Malato S (2016) Pilot-plant evaluation of TiO_2 and TiO_2-based hybrid photocatalysts for solar treatment of polluted water. J Hazard Mater 320:469–478

Anwer H, Mahmood A, Lee J, Kim KH, Park JW, Yip ACK (2019) Photocatalysts for degradation of dyes in industrial effluents: opportunities and challenges. Nano Res 12:955–972

Arslan-Alaton I, Tureli G, Olmez-Hanci T (2009) Treatment of azo dye production wastewaters using photo-Fenton-like advanced oxidation processes: optimization by response surface methodology. J. Photochem. Photobiol. A: Chem 202:142–153

Balık M, Bulut V, Erdogan IY (2019) Optical, structural and phase transition properties of Cu_2O, CuO and Cu_2O/CuO: their photoelectrochemical sensor applications. Int J Hydrog Energy 44:18744–18755

Baruah M, Supong A, Bhomick PC, Karmaker R, Pongener C, Sinha D (2020) Batch sorption–photodegradation of Alizarin Red S using synthesized TiO_2/activated carbon nanocomposite: an experimental study and computer modelling. Nanotechnol Environ Eng 5:8(2020)

Carp O, Huisman CL, Reller A (2004) Photoinduced reactivity of titanium dioxide. Prog Solid State Chem 32:33–177

Chaudhary N, Balomajumder C (2014) Optimization study of adsorption parameters for removal of phenol on aluminum impregnated fly ash using response surface methodology. J Taiwan Inst Chem Eng 45: 852–859

Chen D, Cheng Y, Zhou N, Chen P, Wang Y, Li K, Huo S, Cheng P, Peng P, Zhang R, Wang L, Liu H, Liu Y, Ruan R (2020) Photocatalytic degradation of organic pollutants using TiO_2-based photocatalysts: a review. J Clean Prod 268:121725

Cheng JN, Zhao LZ, Li GB, Li F, Yao MM (2020) B/Co/Fe tridoped TiO_2/SiO_2 composite films for improved photocatalytic degradation of organic pollutants under visible light. Inorg Chem Commun 119: 108089

Delsouz Khaki MR, Shafeeyan MS, Raman AAA, Daud WMAW (2018) Evaluating the efficiency of nano-sized Cu doped TiO_2/ZnO photocatalyst under visible light irradiation. J Mol Liq 258:354–365

Dong H, Zeng G, Tang L, Fan C, Zhang C, He X, He Y (2015) An overview on limitations of TiO_2-based particles for photocatalytic degradation of organic pollutants and the corresponding countermeasures. Water Res 79:128–146

Etacheri V, Di Valentin C, Schneider J, Bahnemann D, Pillai SC (2015) Visible-light activation of TiO_2 photocatalysts: advances in theory and experiments. J Photochem Photobiol C: Photochem Rev 25:1–29

Ferreira SLC, Bruns RE, Ferreira HS, Matos GD, David JM, Brandão GC, da Silva EGP, Portugal LA, dos Reis PS, Souza AS, dos Santos WNL (2007) Box-Behnken design: an alternative for the optimization of analytical methods. Anal Chim Acta 597:179–186

Ganesh I, Kumar PP, Annapoorna I, Sumliner JM, Ramakrishna M, Hebalkar NY, Padmanabham G, Sundararajan G (2014) Preparation and characterization of Cu-doped TiO_2 materials for electrochemical, photoelectrochemical, and photocatalytic applications. Appl Surf Sci 293:229–247

Gaya UI, Abdullah AH (2008) Heterogeneous photocatalytic degradation of organic contaminants over titanium dioxide: a review of fundamentals, progress and problems. J Photochem Photobiol C-Photochem Rev 9:1–12

Gilja V, Katancic Z, Krehula LK, Mandic V, Hrnjak-Murgic Z (2019) Eflciency of TiO_2 catalyst supported by modified waste fly ash during photodegradation of RR45 dye. IEEE J Sel Top Quantum Electron 26:292–300

Giwa A, Yusuf A, Balogun HA, Sambudi NS, Bilad MR, Adeyemi I, Chakraborty S, Curcio S (2021) Recent advances in advanced oxidation processes for removal of contaminants from water: A comprehensive review. Process Saf Environ Prot 146:220–256

Gopinath KP, Madhav NV, Krishnan A, Malolan R, Rangarajan G (2020) Present applications of titanium dioxide for the photocatalytic removal of pollutants from water: a review. J Environ Manag 270:110906

Jin Y, Wu Y, Cao J, Wu Y (2014) Optimizing decolorization of Methylene Blue and Methyl Orange dye by pulsed discharged plasma in water using response surface methodology. J Taiwan Inst Chem Eng 45:589–595

Joo Kim H, Raj Pant H, Hee Kim J, Jung Choi N, Sang Kim C (2014) Fabrication of multifunctional TiO_2-fly ash/polyurethane nanocomposite membrane via electrospinning. Ceram Int 40:3023–3029

Jorfi S, Mirali S, Mostoufi A, Ahmadi M (2018) Visible light photocatalytic degradation of azo dye and a real textile wastewater using Mn, Mo, La/TiO_2/ac nanocomposite. Chem Biochem Eng Q 32:215–227

Kanakaraju D, Wong SP (2018) Photocatalytic efficiency of TiO_2 biomass loaded mixture for wastewater treatment. J Chemother 2018: 4314969

Kanakaraju D, Ravichandar S, Lim YC (2017) Combined effects of adsorption and photocatalysis by hybrid TiO_2/ZnO-calcium alginate beads for the removal of copper. J Environ Sci (China) 55:214–223

Kanakaraju D, Shahdad NRBM, Lim YC, Pace A (2018a) Magnetic hybrid TiO_2/Alg/FeNPs triads for the efficient removal of methylene blue from water. Sustain Chem Pharm 8:50–62

Kanakaraju D, Soon Pang W, Wan Abu Bakar WA (2018b) Photo-fenton treatment of sago wastewater: RSM optimization and toxicity evaluation. J Teknol 80:153–163

Kanakaraju D, Bin Ya MH, Lim YC, Pace A (2020) Combined Adsorption/Photocatalytic dye removal by copper-titania-fly ash composite. Surf Interfaces 19:100534

Kaushik P, Malik A (2011) Process optimization for efficient dye removal by Aspergillus lentulus FJ172995. J Hazard Mater 185:837–843

Khosravi M, Arabi S (2016) Application of response surface methodology (RSM) for the removal of methylene blue dye from water by nano zero-valent iron (NZVI). Water Sci Technol 74:343–352

Körbahti BK, Tanyolaç A (2008) Electrochemical treatment of simulated textile wastewater with industrial components and Levafix Blue CA reactive dye: optimization through response surface methodology. J Hazard Mater 151:422–431

Kumaravel V, Mathew S, Bartlett J, Pillai SC (2019) Photocatalytic hydrogen production using metal doped TiO_2: a review of recent advances. Appl. Catal. B: Environ 244:1021–1064

Luévano-Hipólito E, Torres-Martínez LM, Cantú-Castro LVF (2019) Self-cleaning coatings based on fly ash and bismuth-photocatalysts: Bi_2O_3, $Bi_2O_2CO_3$, BiOI, $BiVO_4$, $BiPO_4$. Constr Build Mater 220: 206–213

Moztahida M, Lee DS (2020) Photocatalytic degradation of methylene blue with P25/graphene/polyacrylamide hydrogels: optimization using response surface methodology. J Hazard Mater 400:123314

Muhd Julkapli N, Bagheri S, Bee Abd Hamid S (2014) Recent advances in heterogeneous photocatalytic decolorization of synthetic dyes. Sci World J 2014:Article ID 692307

Najafi H, Farajfaed S, Zolgharnian S, Mosavi Mirak SH, Asasian-Kolur N, Sharifian S (2021) A comprehensive study on modified-pillared clays as an adsorbent in wastewater treatment processes. Process Saf Environ Prot 147:8–36

Pant B, Ojha GP, Kim HY, Park M, Park SJ (2019) Fly-ash-incorporated electrospun zinc oxide nanofibers: potential material for environmental remediation. Environ Pollut 245:163–172

Pava-Gómez B, Vargas-Ramírez X, Díaz-Uribe C (2018) Physicochemical study of adsorption and photodegradation processes of methylene blue on copper-doped TiO_2 films. J. Photochem. Photobiol. A: Chem 360:13–25

Pedroza-Herrera G, Medina-Ramírez IE, Lozano-Álvarez JA, Rodil SE (2020) Evaluation of the photocatalytic activity of copper doped TiO_2 nanoparticles for the purification and/or disinfection of industrial effluents. Catal Today 341:37–48

Qian S, Pu S, Zhang Y, Wang P, Bai Y, Lai B (2021) New insights on the enhanced non-hydroxyl radical contribution under copper promoted TiO_2/GO for the photodegradation of tetracycline hydrochloride. J Environ Sci (China) 100:99–109

Reza KM, Kurny ASW, Gulshan F (2017) Parameters affecting the photocatalytic degradation of dyes using TiO_2: a review. Appl Water Sci 7:1569–1578

Rtimi S, Pulgarin C, Robyr M, Aybush A, Shelaev F, Gostev F, Nadtochenko V, Kiwi J (2017) Insight into the catalyst/photocatalyst microstructure presenting the same composition but leading to a variance in bacterial reduction under indoor visible light. Appl. Catal. B: Environ 208:135–147

Shafei A, Sheibani S (2019) Visible light photocatalytic activity of Cu doped TiO_2-CNT nanocomposite powder prepared by sol–gel method. Mater Res Bull 110:198–206

Shan R, Lu L, Gu J, Zhang Y, Yuan H, Chen Y, Luo B (2020) Photocatalytic degradation of methyl orange by Ag/TiO_2/biochar composite catalysts in aqueous solutions. Mater Sci Semicond Process 114:105088

Shijitha T, Baiju KV, Shukla S, Patil K, Warrier KGK (2009) Novel electroless process for copper coating of flyash using titania/ultraviolet-radiation/metal catalyst-system. Appl Surf Sci 255:6696–6704

Talebi S, Chaibakhsh N, Moradi-Shoeili Z (2017) Application of nanoscale ZnS/TiO_2 composite for optimized photocatalytic decolorization of a textile dye. J Appl Res Technol 15:378–385

Visa M, Bogatu C, Duta A (2015a) Tungsten oxide - fly ash oxide composites in adsorption and photocatalysis. J Hazard Mater 289:244–256

Visa M, Isac L, Duta A (2015b) New fly ash TiO_2 composite for the sustainable treatment of wastewater with complex pollutants load. Appl Surf Sci 339:62–68

Xin B, Wang P, Ding D, Liu J, Ren Z, Fu H (2008) Effect of surface species on Cu-TiO_2 photocatalytic activity. Appl Surf Sci 254: 2569–2574

Xu J, Sun X, Shan Y, Xu J, Wang G, Wang L (2019) Enhanced UV-light driven photocatalytic performances and recycling properties of TiO_2/AlON composite photocatalyst. Ceram Int 45:6767–6773

Yu L, Xi J, Li M-D, Chan HT, Su T, Phillips DL, Chan WK (2012) The degradation mechanism of methyl orange under photo-catalysis of TiO_2. Phys Chem Chem Phys 14:3589–3595

Yu J, Kiwi J, Wang T, Pulgarin C, Rtimi S (2019) Evidence for a dual mechanism in the TiO_2/CuxO photocatalyst during the degradation of sulfamethazine under solar or visible light: critical issues. J Photochem Photobiol A Chem 375:270–279